Dalton Transactions

PAPER

View Article Online
View Journal

Cite this: DOI: 10.1039/c8dt03905d

The influence of Zn^{II} coordination sphere and chemical structure over the reactivity of metallo-β-lactamase model compounds†

Eduardo Guimarães Ratier de Arruda, [a] Bruno Alves Rocha,[a] Manoel Victor Frutuoso Barrionuevo,[a] Heiðar Már Aðalsteinsson,[a] Flávia Elisa Galdino,[a] Watson Loh, [a] Frederico Alves Lima [b] and Camilla Abbehausen *[a]

A systematic study of the influence of the first coordination sphere over the reactivity and structure of metallo-β-lactamase (MβL) monozinc model complexes is reported. Three Zn^{II} complexes with tripodal ligands forming the series [Zn(N-NNN)], [Zn(N-NNS)], and [Zn(N-NNO)] where N-NNX represents the tripodal donor atoms were investigated regarding their ability to mimic MβL. The tripodal series was inspired by MβL active sites in the respective subclasses, representing the (His, His, His) Zn1 site present in B1 and B3 subclasses, (His, His, Asp) present in the B3 subclass site and the thiolate present in B1 and B2 sites. The results were supported by electronic structure calculations. XAS analysis demonstrated that the Zn^{II} electronic deficiency significantly changes in the order [Zn(N-NNS)] < [Zn(N-NNN)] < [Zn(N-NNO)]. This effect directly affects the reactivity over nitrocefin and amoxicillin, observed by the hydrolysis kinetics, which follows the same trend. NMR spectroscopy revealed the coordination of the carboxylic group in the substrate to the metal changes accordingly, affecting the hydrolysis kinetics. Our results also demonstrated that not only the Lewis acidity is changed by the ligand system but also the softness of the metal. [Zn(N-NNS)] is softened by the thiolate, promoting the ligand substitution reaction with solvents and favoring a secondary interaction with substrates, not observed for [Zn(N-NNO)]. XRD of the models reveals their similar geometric aspects in comparison to the crystal structure of GOB MβL. The present work demonstrates that the Zn^{II} electronic details must be considered in the design of new MβL models that will further aid in the design of clinically useful inhibitors.

Received 27th September 2018,
Accepted 27th October 2018

DOI: 10.1039/c8dt03905d

rsc.li/dalton

1. Introduction

β-Lactam antibiotics are among the most used antibacterial agents and a rising incidence of resistance to these compounds is a public health concern.[1–3] Among several mechanisms of resistance developed by bacteria, the chemical inactivation of the β-lactam drug is one of the most relevant and requires medical and scientific community attention.[4–6] Hydrolysis of the β-lactam ring is catalyzed by enzymes called β-lactamases (βL). Several β-lactamase structures were determined and classified into A, B, C and D classes. The classes A, C and D are serine-based hydrolases and class B is constituted of zinc(II) hydrolases, called metallo-β-lactamases (MβL).[1,7] One strategy to overcome this kind of resistance in the clinic is to combine one inhibitor with a β-lactam antibacterial agent, for example the combined treatment with amoxicillin and clavulanic acid. This strategy was successfully applied to classes A, C and some D β-lactamase producing strains. However, no inhibitors are available for class B, the MβL.[1,8–13]

Although MβLs are very sequence diverse they are structurally similar, presenting a characteristic αβ/βα sandwich fold with the active site located at the interface between domains. The active site can coordinate one or two zinc ions that are central to the catalytic mechanism.[1,14,15] MβLs are divided into three subclasses (B1, B2, B3) based on the primary amino acid sequence homology. Although a small sequence identity is found among subclasses, within each subclass the sequence identity is significant, along with distinctive structural characteristics within the active site of B1, B2 and B3 structures.[14,16,17] Fig. 1 shows the differences in the active site among the subclasses.

It is important to note that even though the active sites among subclasses are structurally similar, these zinc-binding motifs around the active site can distinguish MβL subgroups

[a]University of Campinas, Campinas, P.O. Box 6154, 13083-970, Brazil. E-mail: camabbehausen@iqm.unicamp.br; Tel: +55 19 3251 3055
[b]European X-Ray Free-Electron Laser Facility GmbH, Holzkoppel 4, 22869 Schenefeld, Germany

†Electronic supplementary information (ESI) available. CCDC 1845661. For ESI and crystallographic data in CIF or other electronic format see DOI: 10.1039/C8DT03905D

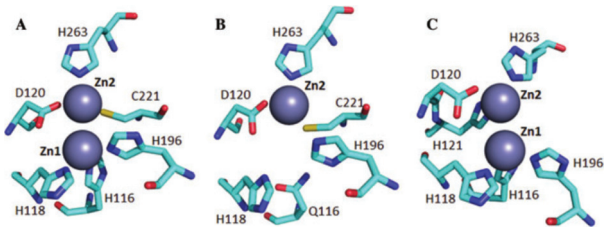

Fig. 1 Schematic illustration of the residues that coordinate Zn(II) in the MβL sites for (a) B1, (b) B2 and (c) B3. The indicated structures correspond to PDB files 1ZNB,[18] 1X8G[19] and 1SML[20] for MBL B1, B2 and B3, respectively. Solvent molecules were hidden.

as B1 (zinc ligands at H116-H118-H196 and D120-C221-H263), B2 (N116-H118-H196 and D120-C221-H263), or B3 enzymes (H/G116-H118-H196 and D120-H121-H262). The distinct amino acid sequences of the subclasses are reflected in somewhat different catalytic properties of the enzymes and in practical terms in the spectrum of action.[1,2]

Over the last few years, a great effort has been devoted to the development of zinc complexes as mimics of MβL entities.[2,21] Detailed studies of mono- and dizinc(II) complexes have led to an understanding of the structural, spectroscopic and mechanistic properties of these systems.[2] Lippard and coworkers pioneered the study of penicillin G and nitrocefin hydrolysis by mono- and dinuclear zinc complexes.[22,23] They successfully mimicked the dinuclear zinc environment of enzymes using two ethylenediamine chelating ligands, allowing the bridging hydroxide to reproduce the nucleophilic attack on the amide bond and also used phenolate bridging ligands to reproduce the Zn^{II} environment. Although a valuable amount of information was generated by these studies, notably regarding the intermediates and single steps of the proposed catalytic mechanism, ligand systems for dinuclear complexes have been designed to conserve a stable dinuclear complex and to prevent the loss of zinc ions. Thus, the hydroxo bridge shows a low nucleophilicity and restrains the mobility between zinc ions.[24] In the flexible native dinuclear enzymes, the binding of the substrate detaches the bridged hydroxide, generating a monocoordinated strong nucleophile. The models developed so far were not able to mimic this step and this might explain why mononuclear models are almost as reactive as dinuclear complexes in these studies.[25–27] In addition, ligand systems are N-donor based and do not consider the differences in the Zn^{II} electronic density (Lewis acidity) caused by aspartate (O-donor) or cysteine (S-donor) coordination in native MβLs.[17]

An important step in the β-lactam hydrolysis mechanism is the coordination of the carboxylate, neighbor to the amide bond in the β-lactam ring, to the metal as revealed by the studies with dinuclear models and by the crystal structure of NDM-1 with hydrolyzed ampicillin.[1] This coordination was previously found to be dependent on the electronic distribution around the zinc ion.[28] As a closed shell (d^{10}) post-transition metal, the electronic density over zinc atoms is mostly modulated by the ligand system and affected by the donor moieties directly coordinated to it, the ligand choice being the key for zinc complex reactivity and motivating this present work.[2] In this study, we systematically investigated the presence of S-donors and O-donors in monozinc MβL model complexes in an attempt to simulate the Zn^{II} different acidities in the three MβL subclasses. The compounds were subjected to X-ray absorption spectroscopy (XAS) combined with time-dependent density functional theory (TDDFT) calculations, NMR spectroscopy investigations of coordination, pseudo-first order kinetics of nitrocefin hydrolysis and isothermal calorimetric studies (ITC). The structural and geometric comparison was mainly focused on the B3 subclass in order to compare a native enzyme with both NNN and NNO homologue sites. The combination of these results demonstrated the importance of the design of the Zn^{II} first coordination sphere and geometric structure in the development of new models for MβL that can further be used for inhibition assays and understanding the inhibition process.

2. Experimental

2.1. General considerations

2-Pyridinecarboxaldehyde (99%), ethyl glycinate hydrochloride (≥98.5%), 2-(aminomethyl)pyridine (99%), sodium borohydride (99%), 2,2,2-trifluoroethanol (≥99%), sodium cyanoborohydride (95%), ethylene sulfide (98%), zinc chloride (≥98.5%), ammonium hexafluorophosphate (≥95%), zinc nitrate hexahydrate (98%) and silica gel for flash chromatography (pore size 60 Å, 220–440 mesh particle size) were purchased from Sigma Aldrich. Nitrocefin (≥95%, batch 0472663-2) was purchased from Cayman Chemicals. Methanol, ethanol, acetic acid, hydrochloric acid, diethyl ether (Et_2O), benzene, ethyl acetate, dichloromethane, chloroform, potassium carbonate (99.5%), sodium sulfate (99%), potassium hydroxide (85%) and dimethylsulfoxide (99%) were purchased from Vetec-Sigma (Brazil). Benzene was treated with P_2O_5 overnight, distilled and freshly distilled from Na/benzophenone. Dimethylsulfoxide was dried over 4A sieves.[29] All reagents were used as received from commercial sources, with no further purification, except when noted. Di(2-pyridylmethyl)amine, tri(2-pyridylmethyl)amine (NNN), *N*,*N*-di(2-pyridylmethyl)aminoethanethiol (NNS), ethyl *N*,*N*-di(2-pyridylmethyl)glycinate (NNOEt), chloro-*N*,*N*-di(2-pyridylmethyl)aminoethanethiolatezinc(II) ([Zn(NNS)]) and the nitrate of diacqua-*N*,*N*-di(2-pyridylmethyl)glycinatezinc(II) [Zn(NNO)] were synthesized using procedures previously described in the literature.[30–34]

2.1.1. Physical measurements. Electronic spectra in the 190–1100 nm range were acquired by using a 10 mm quartz cuvette (1 mL volume) in a diode array HP8453 UV/Visible absorption spectrophotometer equipped with a HP89090A Peltier thermostat. Electrospray ionization mass spectrometry (ESI-MS) measurements were carried out using a Waters Quattro Micro API. Samples were evaluated in the positive mode in an 1 : 1 methanol : water solution with addition of

0.10% (v/v) formic acid. Elemental analyses for carbon, hydrogen and nitrogen were performed using a PerkinElmer 2400 CHN analyzer. ^{1}H and ^{13}C NMR spectra were acquired in deuterated acetonitrile (CD_3CN and dimethylsulfoxide DMSO) solutions using Bruker 250 MHz (5.9 T) and Avance III 400 (9.4 T) spectrometers which were referenced to the signal of tetramethylsilane.[35] The crystallographic measurements were performed with a Bruker Kappa APEX II Duo diffractometer with Mo-Kα radiation (λ = 0.71073 Å). The measurement was made at 150 K using an Oxford Cryostream 700 cryostat. The structure was solved and refined using SHELXL97.[36] ORTEP diagrams were generated using PLATON.[37]

2.2. Ethyl *N*-(2-pyridylmethyl)glycinate synthesis

A new synthetic route was used for the direct reductive amination by using fluorinated alcohol.[38,39] Briefly, in a 25 mL round-bottom flask, 5 mL of 2,2,2-trifluoroethanol and 475.6 μL (5 mmol) of 2-pyridinecarboxaldehyde, freshly distilled under reduced pressure, were added and stirred for 10 min at 45 °C. Subsequently, 697.9 mg (5 mmol) of ethyl glycinate hydrochloride, 622 mg (4.5 mmol) of K_2CO_3 and 5 ml of 2,2,2-trifluoroethanol were added and left under vigorous stirring for 3 hours at 45 °C. After 3 hours, the temperature was reduced to 0 °C and 454 mg (12 mmol) of $NaBH_4$ was added and the mixture was kept overnight under stirring at room temperature. Then, the solvent was removed under reduced pressure and the product was dissolved in 20 mL of $CHCl_3$ and extracted with 3 portions of 20 mL of H_2O. The organic phase was dried with Na_2SO_4 and the solvent was removed. The product was obtained as a yellow oil with a 40% yield. ESI-(+)-MS (MeOH) *m*/*z*: 195 $[(C_8H_9N_2O_2)^+H]^+$. ^{1}H RMN (250 MHz, CD_3CN) σ (ppm): 8.46 (m, 1H), 7.70 (m, 1H), 7.45 (m, 1H), 7.19 (m, 1H), 4.12 (q, 2H, J = 7.3 Hz), 3.86 (s, 2H), 3.39 (s, 2H) e 1.20 (t, 3H, J = 7.3 Hz).

2.3. Chloro-tri(2-pyridylmethyl)aminezinc(II) hexafluorophosphate synthesis

The complex was synthesized using an adapted procedure described by Xu *et al.*[40] In a 50 mL round-bottom flask, a 10 mL methanolic solution containing 145.2 mg (0.5 mmol) of tri(2-pyridylmethyl)amine (N-NNN) was mixed with 5 mL of a methanolic solution containing 68.2 mg (0.5 mmol) of $ZnCl_2$. The solution was stirred at room temperature for 3 hours. Then, the volume was reduced (~4 mL) and 1 mL of a saturated methanolic solution of NH_4PF_6 was added. A light-yellow powder was obtained and washed with water followed by Et_2O. Single crystals suitable for XRD were obtained by diffusion of Et_2O in a diluted methanolic solution of the complex. The product was obtained as a light-yellowish powder with 76% yield.

Anal. calc. for $[Zn(C_18H_18N_4)Cl](PF_6).(H_2O)_3$: C 36.63; H 4.09; N 9.49; found: C 36.26; H 3.15; N 9.43. ESI-MS (MeOH) *m*/*z*: 399.5 $[Zn(NNN)(HCO_2)]^+$ and 389.4 $[Zn(NNN)(Cl)]^+$. ^{1}H NMR (250 MHz, CD_3CN) σ (ppm): 9.01 (m, 3H), 8.06 (m, 3H), 7.62 (m, 3H), 7.53 (m, 3H) e 4.18 (s, 6H). ^{13}C NMR (62.9 MHz, CD_3CN) σ (ppm): 156.2; 149.7; 142.4; 126.2; 125.7 e 57.6.

2.4. Nitrocefin hydrolysis assay

For nitrocefin hydrolysis kinetic assays, stock solutions of nitrocefin (0.2 mmol L^{-1}) and [Zn(N-NNX)], with X = S, N or O, complexes (5 mmol L^{-1}) were prepared, ensuring that the solids were completely soluble. A solution, 2 : 8 ratio phosphate buffer pH 7.4 (50 mmol L^{-1}): DMSO was used as a solvent. Prior to use, the solvent was filtered using a 0.22 μm syringe filter. All solutions were prepared using the same solvent and measured at 40 °C. A blank spectrum was acquired using solely the solvent.

In a test tube, 80 μL of the complex stock solution and 520 μL of solvent were added. Prior to the kinetic measurement, 200 μL of the nitrocefin stock solution was added and the mixture was stirred for 5 seconds. The initial concentrations of $[Nitrocefin]_{initial} = 5.0 \times 10^{-5}$ mol L^{-1} and $[Zn(N\text{-}NNX)] = 5.0 \times 10^{-4}$ mol L^{-1}.

After stirring, the solutions were transferred to a 1000 μL quartz cuvette with 1 cm optical path. The cuvette was placed in the spectrophotometer for 60 seconds for temperature stabilization. Then, spectra in the range of 300–800 nm were acquired every 20 seconds for 7200 seconds, with a resolution and step size of 1 nm. The experiment was performed in duplicate.

In order to obtain a pseudo-first order ratio kinetics depending on the nitrocefin concentration, the experiment was repeated in four nitrocefin concentrations in the range of $[Nitrocefin]_{initial} = 2.5 \times 10^{-5}$ to 6.25×10^{-5} mol L^{-1}. The absorbance values were measured at 562 nm (absorbance maximum of the hydrolyzed product) and hydrolysis activity values were obtained using the model proposed by Kaminskaia *et al.* with a maximum conversion of 15%.[22,23] The molar absorptivity at 562 nm of hydrolyzed product and the nitrocefin in this solvent was previously determined and the values of $\varepsilon_{hydrolized} = 1052$ cm^{-1} mol^{-1} L and $\varepsilon_{nitrocefin} = 428$ cm^{-1} mol^{-1} L were obtained.

2.5. Interaction of the complexes with KOAc or amoxicillin

The amoxicillin interaction was based on similar experiments conducted by Kaminskaia *et al.*[22] In order to evaluate the metal Lewis acidity and amoxicillin interaction, a stock solution of concentration 9.14×10^{-2} mol L^{-1} of the substrate (potassium acetate or amoxicillin) in d_6-DMSO was prepared. To 750 μL d_6-DMSO solution containing the compounds investigated here ([Zn(N-NNO)], [Zn(N-NNN)] and [Zn(N-NNS)]) in a concentration of 4.57×10^{-6} mol L^{-1}, 50 μL of the substrate stock solution was added, resulting in an equimolar concentration of 5.71×10^{-3} mol L^{-1}. ^{1}H NMR spectra of the pure compounds and the mixtures were acquired. In the case of mixtures, the spectra were obtained and followed for 30 minutes.

2.6. X-ray absorption spectroscopy

The solid samples of the three zinc complexes used in the XAS measurements were finely ground and diluted in boron nitride to a calculated maximum X-ray absorbance of about 1. They

were then pressed into circular pellets of 13 mm diameter and about 1 mm thickness using a hydraulic press, placed in a plastic sample holder and covered with polyimide adhesive tape (Kapton) with about 40 μm thickness. Data averaging, background subtraction and normalization were done using standard procedures as implemented in the DEMETER package.[41]

Zinc K-edge XAS spectra were obtained at XAFS1 and XAFS2 beamlines, both located at the Brazilian Synchrotron Light Laboratory (CNPEM/LNLS).[42,43] At the XAFS1 beamline the incident energy was selected by a channel-cut monochromator equipped with a Si(220) crystal, and at the XAFS2 beamline, a fixed-exit monochromator was used. The beam size at the sample was approximately 2.5 × 0.5 mm^2 (hor. × vert.) at XAFS1 and 0.4 × 0.4 mm^2 at XAFS2, with an estimated X-ray flux of 10^8 ph s^{-1} (XAFS1) and 10^9 ph s^{-1} (XAFS2). The incoming X-ray energy was calibrated by setting the maximum of the first derivative of the K-edge XAS spectrum of a zinc metal foil to 9659 eV. The XAS spectra were obtained in conventional transmission mode using ion chambers filled with a mixture of He and N_2.

2.7. Theoretical studies

All computations were carried out using Orca 4.0.1 software developed by Neese and coworkers.[44] Structures were optimized using the PBE0 functional and def2-TZVP basis set[45] using the crystal structures as a starting point.[33,34] All structural analyses were performed by using PyMOL (version 1.7.2.1).[46] The GOB-18 crystal structure (PDM ID 5K0W) and L1 crystal structure (PDB ID 1SML) were collected from the Protein Data Bank (PDB). The enzyme pocket was extracted by selecting all residues inside a radius of 4 Å from the zinc metal ion. The enzyme pocket extraction was able to pick both sites that comprise the pocket, site 1 that is composed of three histidines and site 2 that is composed of two histidines and one aspartic acid.

TDDFT calculations for the K-edge transitions were made for [Zn(NNX)], with X = O, N and S, complexes in order to assign the pre-edges observed in the XAS experiments for these compounds. They were performed on the DFT optimized structures and the crystal structures, where only hydrogen atoms were optimized. The PBE0 functional was also used in TDDFT calculations by employing the Tamm–Dancoff and RIJCOSX approximations.[47–49] The relativistic Douglas–Hess–Kroll Hamiltonian was used with the DKH-def2-TZVP basis set and SARC/J auxiliary basis set as implemented in ORCA 4.0.1.[50–52] Calculations were carried out using the conductor like polarizable continuum solvation model (CPCM) with an infinite dielectric.[53] Transitions were allowed from the Zn 1s orbital into all of the unoccupied orbital space. Up to 200 roots were calculated. The calculated transitions were convoluted with a 1.7 eV FWHM Gaussian to match the experimental resolution.[54] TDDFT is known to have systematic errors leading to inaccurate absolute energies.[55–57] Therefore, a constant different energy shift (93.5 eV) was applied to all spectra to align theory with experiment.

2.8. Fukui indexes

Fukui indexes can be computed by using a condensed method,[58,59] the equations depicted below summarize this methodology:

$$f^{-}(i) = q_N(i) - q_{N-1}(i) \quad (1)$$

$$f^{+}(i) = q_{N+1}(i) - q_N(i) \quad (2)$$

where q stands for the charge of atom i in an unperturbed system (N), *i.e.*, where an electron has neither been removed ($N-1$) nor added ($N+1$).

For each previously optimized zinc complex, a sequence of three single-point runs was performed by employing the PBE functional, def2-TZVP basis set, and Grimme's dispersion correction (D3BJ).[45,60] The first single-point corresponds to the complex not perturbed, the second is perturbed by adding an electron and the third by removing an electron. These computations were repeated, using the PBE0 functional. Atomic charges were obtained from Hirshfeld Population Analysis (HPA)[61] and Natural Population Analysis (NPA).[62] The latter was computed using the JANPA software,[63] while the former was obtained using the ORCA software. The values for Fukui indices were taken only for the Zn^{II} metal ion.

2.9. Isothermal titration calorimetry, ITC

Calorimetric measurements were carried out using a MicroCal VP-ITC (Northampton, MA, USA). The syringe and the sample cell were loaded with 280 μL amoxicillin (9.650 mM) and 1.43 mL Zn complex (0.799 mM), respectively. All solutions were prepared in DMSO. Small aliquots ranging from 4–10 μL of amoxicillin were injected into the sample cell. Control experiments were carried out by titrating amoxicillin into DMSO. A constant stirring at 307 rpm was used and the time between injections was 300 s. All measurements were performed at 298 K and in triplicate.

Data were analyzed using the one set of sites model implemented in the Origin 7.0 software provided with the MicroCal VP-ITC.[64] The standard molar enthalpy change (ΔH), equilibrium constant (K) and stoichiometry were obtained directly from the fit. The molar Gibbs free energy change (ΔG) and molar entropy change (ΔS) were calculated based on K and ΔH values.

3. Results and discussion

3.1. Structure and coordination sphere of the synthetic models

An investigation of the influence of the zinc first coordination sphere on the ability to mimic MβL active sites was done using the three tripodal compounds shown in Fig. 2a–c, the fourth complex is also included, as seen in Fig. 2d, and a previously studied dizinc complex [ZnZn] in our investigation as a comparison with literature models.[65] The set of ligands also mimics the coordination of charged residues to zinc, changing significantly the overall charge of the complex. Cysteines coordinate to zinc as thiolates affecting the metal charge. The

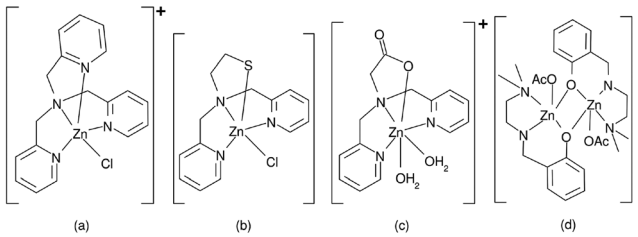

Fig. 2 Zn^{II} complexes proposed as MβL mimetics, named according to the donor atoms of the tripodal ligands and one standard model: (a) [Zn(N-NNN)], (b) [Zn(N-NNS)], (c) [Zn(N-NNO)] and (d) [ZnZn].[65]

aspartate in the [Zn(N-NNO)] mimics the presence of essential Asp120, which is showed to stabilize Zn^{II} as a strong zinc ligand optimizing the substrate binding.[66] Also, it is responsible for the inactivation of the enzyme at acidic pH.[67] Tripodal ligands were obtained by modifications of tri-(2-pyridylmethylamine) and are called here by the donor atoms as N-NNN (tri-(2-pyrididylmethylamine), *N*,*N*-di(2-pyridylmethyl)aminoethanethiol (N-NNS), and *N*,*N*-di(2-pyridylmethyl)glycinate (N-NNO). Out of the four compounds in our study three are tripodal monozinc complexes, namely [Zn(N-NNO)], [Zn(N-NNN)], and [Zn(N-NNS)]. N- represents the amine, common in the three complexes, and is the center of the arms of the tripodal system, N-NNX, the other two N represent the pyridil moieties, and X is the variable moiety N (pyridyl), O (carboxylate) and S (thiolate). In the literature a diversity of Zn^{II} complexes were evaluated as MβL models, however studies trying to correlate the structure and reactivity of these mimetics are rare.[2]

A new [Zn(N-NNN)] complex, with a PF_6^- counter-ion, was synthesized using an adapted methodology[40] and the other three compounds were synthesized as previously described.[33,34,65] All ligands and complexes were characterized using spectroscopic (^1H and ^{13}C NMR) and spectrometric analyses, in agreement with previous characterization studies.[30–34,65] In the case of [Zn(N-NNS)], [Zn(N-NNN)] and [ZnZn] the structures were obtained using single-crystal X-ray diffraction. The structure obtained was consistent with that previously found in the literature.[33,65] The crystallization of [Zn(N-NNO)] did not result in crystals suitable for single crystal XRD, and for the comparative structural analysis, the data obtained by Abufarag *et al.* were used.[34] The [Zn(N-NNN)] complex was crystallized and presented a different space group compared to the previously reported structure, however, maintaining comparable distances and angles.[68–70] The structural data for this new crystal were obtained and are presented in Table S1,† the ORTEP figure is shown in ESI Fig. S1.† The crystal data were deposited in The Cambridge Crystallographic Data Center (CCSD).

The [Zn(N-NNN)] compound has a pentacoordinated structure, with the Zn^{II} ion in a trigonal bipyramidal geometry and the cation neutralized by PF_6^- charges. The ligand N-NNN binds to the Zn^{II} by four nitrogens and chloride completes the coordination sphere. As stated above, the crystal structure of [Zn(N-NNN)] obtained by our alternative synthesis method agrees with the one previously obtained for the ion $[Zn(N\text{-}NNN)Cl]^+$, with the bond length of $Zn–N_{py} \approx 2.08$ Å, $Zn–Cl \approx 2.27$ Å and $Zn–N_{am} \approx 2.25$ Å and the angle $Cl–Zn–N_{am} \approx 180°$. The main distances and angles for the XRD structures of [Zn(N-NNN)], [Zn(N-NNO)], [Zn(N-NNS)], and [ZnZn] are shown in Table 1. In the tripodal complexes, the change of the moiety from pyridine to thiolate, in one arm of the tripodal ligand, resulted in bigger $Zn–N_{py}$ distances, 2.075 Å in [Zn(N-NNN)] and 2.109 Å in [Zn(N-NNS)], and Zn–Cl, 2.268 Å in

Table 1 Selected bond distances and angles from the single-crystal XRD of the complexes [Zn(N-NNN)], [Zn(N-NNS)], [Zn(N-NNO)], and ([ZnZn]), with N_{am} being the tertiary amine nitrogen, N_{amsec} being the secondary amine nitrogen, N_{py} being the pyridine nitrogens, O_{phen} being the oxygen in phenolate, O_{H_2O} being the oxygen in the coordinated water and O_{carb} being the oxygen in carboxylate.[33,34,65] For [Zn(NNN)], the distances and angles in this work and ref. 68 are shown side by side

[Zn(N-NNN)]				[Zn(N-NNS)][33]			
Length, Å		Angle (°)		Length, Å		Angle (°)	
$Zn–N_{py}$	2.075(4)/2.074(7)[a]	Cl–Zn–N_{am}	178.1(1)/177.9(2)[a]	$Zn–N_{py}$	2.109(4)	Cl–Zn–N_{am}	168.3(1)
$Zn–N_{am}$	2.258(3)/2.239(7)[a]	Cl–Zn–N_{py}	102.6(1/100.1(2)[a]	$Zn–N_{am}$	2.299(4)	Cl–Zn–N_{py}	99.0(1)
Zn–Cl	2.268(1)/2.271(3)[a]	$N1_{py}$–Zn–$N2_{py}$	117.9(2)/114.9(3)[a]	Zn–Cl	2.342(1)	$N1_{py}$–Zn–$N2_{py}$	115.5(2)
		N_{am}–Zn–N_{py}	77.4(2)	Zn–S	2.312(1)	Cl–Zn–S	105.87(5)
						S–Zn–N_{py}	118.6(1)

[Zn(N–NNO)][34]				[ZnZn][65]			
Length, Å		Angle (°)		Length, Å		Angle (°)	
$Zn–N_{py}$	2.116(4)	O_{carb}–Zn–N_{am}	80.9(1)	$Zn–O_{phen}$	2.033(1)	O_{phen}–Zn–$O1_{phen}$	81.22(5)
$Zn–N_{am}$	2.198(3)	O_{carb}–Zn–N_{py}	92.2(1)	$Zn–O_{carb}$	1.994(1)	O_{phen}–Zn–O_{carb}	99.12(1)
$Zn–O_{carb}$	2.134(3)	$N1_{py}$–Zn–$N2_{py}$	156.2(1)	$Zn–N_{amsec}$	2.126(2)	$N1_{amsec}$–Zn–$N2_{am}$	81.29(6)
$Zn–O_{H_2O}$*trans*\am	2.010(3)	O_{H_2O}*trans*\am–Zn–N_{am}	174.7(1)	$Zn–N_{am}$	2.158(2)	Zn–O_{phen}–Zn1	98.78(5)
$Zn–O_{H_2O}$*trans*\carb	2.244(3)	O_{H_2O}*trans*\carb–Zn–O_{carb}	175.6(1)	Zn–Zn	3.113(1)	N_{am}–Zn–O_{phen}	167.42(6)
		$N1_{am}$–Zn–$N1_{py}$	78.1(1)				

[a] ref. 68.

[Zn(N-NNN)] and 2.342 Å in [Zn(N-NNS)], and smaller angles between the nitrogenated moieties and zinc ($N1_{py}$–Zn–$N2_{py}$), 117.9° in [Zn(N-NNN)] and 115.5° in [Zn(N-NNS)]. These point to the inclusion of a more flexible and bulky ethylthiol group in the vicinity of the zinc atom.[33] The comparison of the octahedral [Zn(N-NNO)] with the other tripodal complexes ([Zn(N-NNN)] and [Zn(N-NNS)]) showed a bigger Zn–N_{py} (2.116 Å) and $N1_{py}$–Zn–$N2_{py}$ (156.2°) than for the [Zn(N-NNN)] and [Zn(N-NNS)] complexes that can be explained by its higher coordination number.

In the MβL active site, the Zn atom can assume different coordination spheres depending on the residues and water molecules present in the pocket.[1] In this sense, the compounds investigated here ([Zn(N-NNO)], [Zn(N-NNN)] and [Zn(N-NNS)]) reveal that small changes in the ligand moieties can lead to a different coordination number and structure for these complexes in the solid state. In the presence of water or other basic solvents, a quick exchange between these molecules and the monodentate ligands (chloride in [Zn(N-NNN)] and [Zn(N-NNS)], and coordinated water molecules in [Zn(N-NNO)]) is observed by NMR (Fig. S5–S7†) and MS experiments in agreement with other Zn^{II} MβL models.[2,22,23,33] In solution, the ligand exchange is going to cause charge variation, depending on the solvent employed. The coordination of water is critical, and the formation of hydroxide cannot be disregarded in this case. In order to study the interaction with the substrate, dried solvents were used to avoid substrate hydrolysis and the pK_a associated with the coordination of water is a subject for future investigation. Each case and solvent is discussed according to the experiment.

3.2. Structural comparison between synthetic models and a MβL active site

A comparison of coordination geometry was performed in order to evaluate the structural similarities between selected active sites of MβL with the model complexes. For this study we chose GOB-type metallo-β-lactamase from the opportunistic pathogen *Elizabethkingia meningoseptica* (PDB ID 5K0W)[71] and L1 from *Stenotrophonomas maltophilia* (PDB ID 1SML).[20] GOB-18 is a very interesting structure and despite being classified as a B3 subgroup, it has an uncommon behavior for a B3 enzyme as it can show an almost B2-like catalytic activity. As shown by Alejandro J. Vila *et al.*[71] GOB-type enzymes present a hybrid characteristic where it can be fully functional in a mono-zinc form in spite of its amino acid change of His116Gln.[72] The Zn site 1 was structurally compared with [Zn(N-NNN)] and Zn site 2 with [Zn(N-NNO)]. The site 1 has two His and one Gln coordinated and the site 2 has two His and one Asp as illustrated in Fig. 3. On the other hand L1 has the classical B3 structure as represented in Fig. 1c and S2.† The complex [Zn(N-NNS)] does not have similarity regarding the geometry and coordination sphere around the zinc metal with any known MβL, however, it is proposed as a model in order to evaluate the effect of a coordinated thiolate, found in the Zn site 2 of B1 and B2, as cysteine replaces histidine (Fig. 3).

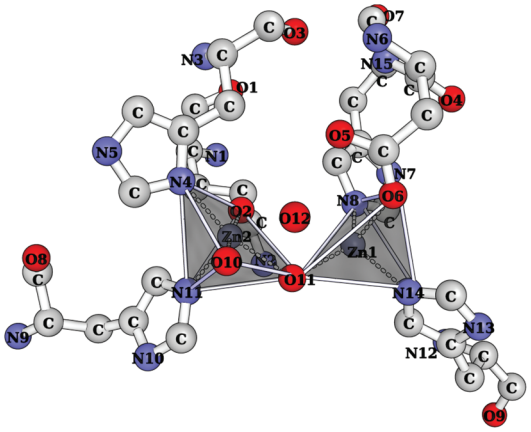

Fig. 3 GOB-18 (5K0W) B3-MβL active sites numbered structure with the zinc atoms coordination sphere highlighted for both of them. The site 1 (Zn1) was compared with the [Zn(N-NNN)] model and the site 2 (Zn2) was compared with [Zn(N-NNO)]. Nitrogen atoms are colored in blue, oxygen atoms in red, zinc in grey and carbon in light grey.[71]

All the experimental evaluations performed in this work were made using diluted solutions of [Zn(N-NNX)] complexes. To simulate the complex structures in solution without the packing effect, DFT optimized structures of the model complexes were used in comparison with the enzyme sites instead of crystal structures. The vacuum calculated geometries were free of the packing effect present in the crystals, mainly due to the counter-ion's proximity and crystalline hydrogen bond interactions, as observed in the [Zn(N-NNO)] structure for the coordinated water.[34] These DFT structures were calculated using the respective crystal structure as the starting point. This structural relaxation can be observed by comparing the py–Zn–py angle that is more constrained (117.9°) for $[Zn(N\text{-}NNN)]_{XRD}$ than for $[Zn(N\text{-}NNN)]_{DFT}$ (119.4°), likely due to the presence of a PF_6^- counter-ion in the vicinity in the solid state (see Fig. S1†). The structural formulas of the DFT optimized complexes of [Zn(N-NNN)], [Zn(N-NNS)] and [Zn(N-NNO)] are shown in Fig. 4a, 4b and 4c. To compare with a classic literature mimetic, the crystal structure of a dizinc complex [ZnZn] (see Fig. 4d) was used.[65]

The structures of the GOB-18 (5K0W) and L1 (1SML) B3-MβL were retrieved from the Protein Data Bank (PDB)[20,71] and their active sites were isolated and are shown in Fig. 3 and S2† respectively. The GOB-18 (5K0W) site 1 is composed of the Zn1 coordinated in a distorted bipyramidal geometry to atoms O11 (water bridge), O10 (water), N4 (His100), N11 (His175), and O2 (Gln98). The site 2 is composed of Zn2 coordinated in a distorted tetrahedral geometry to O11 (water bridge), O6 (Asp84), N8 (His103) and N14 (His241). For the structural comparison, Table 2 depicts the main values of bond lengths and bond angles found for site 1 (similar to [Zn(NNN)]) and site 2 (similar to [Zn(NNO)]) of 5K0W enzyme pocket, as well as for the [Zn(NNN)], [Zn(NNO)] and [ZnZn] complexes.[34]

In the case of L1 (1SML) site 1 is composed of Zn2 coordinated in a distorted bipyramidal geometry to atoms O4

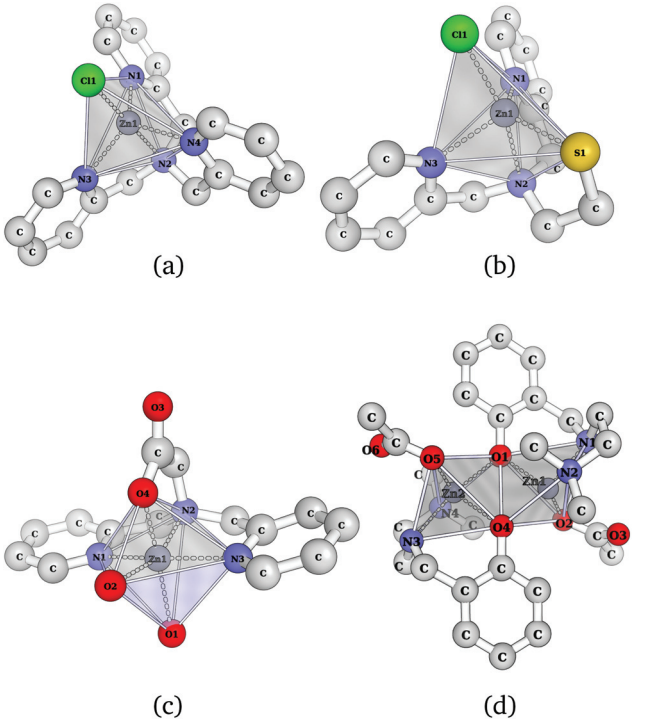

Fig. 4 Numbered DFT optimized structures of the complexes (a) $[ZnCl(N\text{-}NNN)]^+$, (b) [ZnCl(N-NNS)] with the zinc atoms trigonal bipyramidal coordination sphere highlighted. (c) $[Zn(N\text{-}NNO)(H_2O)_2]^+$with the zinc atom octahedral coordination sphere highlighted and (d) [ZnZn] with the zinc atoms square-plane pyramidal coordination sphere highlighted. Nitrogen atoms are colored in blue, sulfur in yellow, chlorine atoms in green, zinc in grey and carbon in light grey. Hydrogen atoms have been removed for clarity.

(water bridge), O3 (water–H-bonded to Ser185 O2), N42 (His89), N62 (His225) and O32 (Asp88). The site 2 is composed of Zn1 coordinated in a distorted tetrahedral geometry to O4 (water bridge), N14 (His84), N21(His86) and N52 (His160). For the structural comparison, Table S2† depicts the main values of bond lengths and bond angles found for site 1 (similar to [Zn(N-NNN)]) and site 2 (similar to [Zn(N-NNO)]) of 1SML enzyme pocket, as well as for the [Zn(N-NNN)] and [Zn(N-NNO)] complexes.[34]

As can be seen in Table 2, the [Zn(N-NNN)] and [Zn(N-NNO)] structures have bond lengths close to that of their related sites of the enzyme GOB-18. The differences observed are in the range of 0.02–0.14 Å and the main deviations are observed in the bond angles (around 10° for N-Zn-N in [Zn(N-NNN)] and 50° in [Zn(N-NNO)]). It is important to consider the macromolecular nature of the enzyme that leads to different constraints in a metal coordination site compared to the constraints present in a small inorganic molecule. Therefore, length and angle deviations are expected when comparing our models with the enzyme active site.[2,73] Besides [Zn(N-NNO)] presents a more similar coordination sphere of both sites, it has a larger N–Zn–N angle than [Zn(N-NNN)]. Overall, [Zn(N-NNN)] is more similar to the sites of GOB-18 with respect to both bond lengths, and angles in the His–Zn bond comparison. The larger deviation of [Zn(N-NNO)] can be explained by geometric constraints caused by chelating effects of the N-NNO ligand, leading to a more hindered coordination of the carboxylate moiety than is observed for the aspartate in the enzyme active site, but keeping a higher similarity for the N–Zn–O angles. On comparing [Zn(N-NNO)] and [Zn(N-NNN)], it is possible to observe that the average Zn–N bond length is larger for [Zn(N-NNO)] than for [Zn(N-NNN)]. This difference is likely due to lower steric hindrance present in the trigonal bipyramidal geometry of [Zn(N-NNN)] that binds the zinc atom

Table 2 Bond lengths and bond angles of [Zn(N-NNN)], [Zn(N-NNO)] optimized by the PBE0 functional, [ZnZn] crystals, and the retrieved 5K0W pocket. See numbered structures in Fig. 4

5K0W pocket[71]		[Zn(N-NNN)]		[Zn(N-NNO)]		[ZnZn][65]	
Measured	Length (Å)	Measured	Length (Å)	Measured	Length (Å)	Measured	Length (Å)
D(Zn2, N14)	2.0767	—	—	D(Zn1, N3)	2.1293	D(Zn1, N1)	2.1259
D(Zn2, N8)	2.0997	—	—	D(Zn1, N7)	2.1146	D(Zn1, N2)	2.1581
D(Zn2, O6)	2.1119	—	—	D(Zn1, O4)	1.9736	—	—
D(Zn2, O11)	2.0623	—	—	—	—	D(Zn1, O1)	2.0331
D(Zn2, Zn1)	3.5155	—	—	—	—	D(Zn1, Zn2)	3.1330
D(Zn1, N11)	2.0618	D(Zn2, N3)	2.0850	—	—	D(Zn2, N4)	2.1581
D(Zn1, O3)	2.0356	D(Zn1, N4)	2.0860	—	—	D(Zn2, O5)	1.9944
D(Zn1, N4)	2.0627	D(Zn1, N1)	2.0863	—	—	D(Zn2, N3)	2.1259
D(Zn1, O11)	2.0750	—	—	—	—	D(Zn2, O1)	2.0935
	Angle (°)		Angle (°)		Angle (°)		Angle (°)
A(N8, Zn2, 14N)	104.1627	—	—	A(N7, Zn1, N3)	155.7314	A(N2, Zn1, N1)	81.2852
A(N8, Zn2, O6)	94.5060	—	—	A(N1, Zn1, O4)	98.6513	—	—
A(O6, Zn2, N14)	98.5882	—	—	A(O4, Zn1, N3)	93.2717	—	—
A(N8, Zn2, O11)	125.6943	—	—	A(N1, Zn1, O2)	95.9252	A(N2, Zn1, O1)	111.0490
A(O3, Zn1, N11)	95.2148	A(N4, Zn1, N3)	113.8002	—	—	A(O5, Zn2, N4)	141.5231
A(N4, Zn1, N11)	103.6364	A(N1, Zn1, N3)	113.8652	—	—	—	—
A(O3, Zn1, N4)	90.8811	A(N4, Zn1, N1)	114.1139	—	—	A(O5, Zn2, N3)	92.8427

more closely than the more hindered octahedral geometry of [Zn(N-NNO)]. In the case of L1 the site 1 has the zinc coordinated to three His, similarly to [Zn(N-NNN)]. The structural comparison of [Zn(N-NNN)] and [Zn(N-NNO)] and L1 (1SML) showed very similar deviations to that observed for GOB-18, with differences in the bond distances of 0.01–0.10 Å but considerably higher deviation in the bond angles (around 20°) as can be seen in Table S2.† Despite the fact that the coordination sphere of L1 is much more similar to the model [Zn(N-NNN)] the models present more similarities to the sites of GOB-18.

Finally, the dizinc complex [ZnZn], Fig. 4d, presented the largest deviation from the measured bond lengths and bond angles with respect to the GOB-18 (5K0W) and L1 (1SML) pocket, which indicates that the dizinc complex has a lower similarity to the enzyme pocket geometry. In the crystal structure, the Zn–Zn distance on the dizinc complex is around 0.38 Å shorter than the GOB-18 and 0.33 Å shorter than L1. Moreover, in this complex, the coordination sphere around zinc atoms keeps neither similar moieties bonded to the metal, with phenoxide and alkyl amines instead of imidazole and water, nor a geometric structure, due to the square-based pyramidal geometry and a rigid phenoxide bridge between the two zinc atoms.[1,2,22,23,65]

3.3. Coordination sphere and influence on the kinetics

3.3.1. Influence of the zinc coordination sphere on the kinetics. To understand the influence of coordination sphere on the reactivity, the kinetics of nitrocefin hydrolysis was conducted aiming to analyze our tripodal Zn^{II} complexes as MβLs models.[22,23] The pseudo-first-order rate constant for this reaction was measured using the hydrolytic conversion of nitrocefin at low conversion (≤15%) and by varying the concentration of the substrate. The experiment was conducted in a low concentration of water, keeping the 2 : 8 buffer : DMSO ratio.[2] The water portion solution had the pH adjusted to 7.4 (buffered). In the conditions of the experiment the labile ligands (chloride and water) must be mostly exchanged by DMSO. The free water might act as a nucleophile as the described mechanism for monozinc.[27,74] Under these conditions we were able to evaluate the influence of coordination sphere over reactivity. Charge effects are also discussed. The obtained values for the reaction rate constants are given in Table 3.

Our experiment points to the dependence of the kinetic rate on ligand set, decreasing in the following order: [Zn(N-NNO)] > [Zn(N-NNN)] > [Zn(N-NNS)]. Considering the ligand exchange of chloride for neutral solvent molecules (DMSO or water) the charges of [Zn(N-NNO)] and [Zn(N-NNS] are 1+ and [Zn(N-NNN)] is 2+. The chloride exchange is well observed for [Zn(N-NNS)Cl] by ^{1}H NMR (Fig. S6†) and is also proposed for the other two complexes as observed by mass spectrometry. No discussion about the effect of overall charge on the kinetics of MBL model complexes is found in the literature. Considering the high ligand lability and charge variation over time of the reaction, mainly with the coordination of the substrate, its hydrolysis and detachment was pointed by Umayal and co workers.[75] In the enzyme as a whole the positioning of the substrate is mostly affected by the surface potential. Here, the fact that [Zn(N-NNN)] can assume a 2+ charge after chloride displacement can affect the rate. However, when compared with the series of complexes no higher deviation is observed suggesting that the overall charge is not the main effect in this case allowing the comparison.

As established in the literature, hydrolysis of β-lactam compounds is activated by the coordination of the β-lactam closest carboxylate, as shown in Fig. 5.[2,22,74] The order observed in the rate constant allows hypothesizing a correlation between zinc electronic density (or its Lewis acidity) and the strength of carboxylate coordination, consequently affecting the hydrolysis rate.[17] The rate is lower in the presence of the thiolate donor and higher in the presence of carboxylate. Thiolates are qualitatively better donors than carboxylates in this case affecting the zinc electronic density.[2,33] This hypothesis is further corroborated by Zn K-edge XAS and DFT data. Also, the presence of thiolate was found to favor a secondary interaction with β-lactams as discussed in the following sections. The overall charge might contribute to the individual reactivity, mainly attraction and positioning of the substrate, however the set of data suggests that it is not the main effect for the trend. These values obtained for the pseudo-first-order kinetic rates constants are comparable with the literature data for mononuclear species as [Zn(cyclen)](NO$_3$)$_2$ (2.8×10^{-3} min^{-1}) and Zn(NO$_3$)$_2$ (1.3×10^{-3} min^{-1}).[2] Therefore, the obtained kinetic rate con-

Table 3 Pseudo-first order kinetic constant (k) and initial rate (v_0) for nitrocefin hydrolysis activated by zinc models in phosphate buffer : DMSO at 40 °C. For [Zn(N-NNX)], with X = O, N and S, the solvent used was 2 : 8 phosphate buffer : DMSO, whereas for [ZnZn], the solvent was used 1 : 9 phosphate buffer : DMSO[65]

Compounds	k (min^{-1})	Error (min^{-1})	v_0 (μmol min^{-1})
[Zn(N-NNO)]	2.5×10^{-3}	0.1×10^{-3}	1.3×10^{-1}
[Zn(N-NNN)]	1.9×10^{-3}	0.2×10^{-3}	6.6×10^{-2}
[Zn(N-NNS)]	1.5×10^{-3}	0.1×10^{-3}	1.6×10^{-2}
[ZnZn][65]	—	—	6.1×10^{-1}

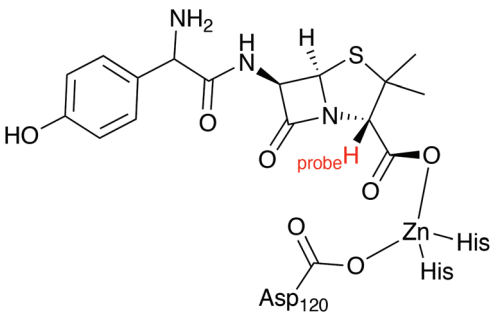

Fig. 5 Molecular structure of amoxicillin in which the geminal hydrogen to the carboxylic acid bonded to the 5-membered ring was used as a probe to evaluate the interaction between it and our zinc models. The literature proposes this carboxylate as the first moiety to coordinate to the Zn^{II} in the active site, as presented by a schematic monozinc active site.[1,2,74]

stants for our zinc models confirm that these complexes are indeed suitable models for MβLs, showing a similar behavior as previously reported complexes.[2] As observed in MβL models literature, dinuclear Zn–Zn complexes usually present a higher hydrolytic rate constant than monozinc complexes. The complex [ZnZn] and their similar literature dizinc models present constants (k) in the range of 5×10^{-3} to 13×10^{-3} min^{-1}.[2,22,23] This is not surprising as the synergistic and cooperative effects found in dizinc compounds are lacking on these models. It is not the aim of this work to make a direct comparison on the activities but contribute to the information already obtained by the dizinc models by studying the influence of S-, N- and O-donor ligands. It is important to highlight the similar order of magnitude between [ZnZn] and [Zn(N-NNO)] showing that our monozinc complexes acts as good MβL models.

3.2. Influence of the coordination sphere of the complexes in the reaction with carboxylates

As previously mentioned, the mechanism of β-lactam hydrolysis by MβL consists of the coordination of carboxylate neighbor to β-lactam ring to the metal ion (Fig. 5). The influence of the coordination sphere in the carboxylate coordination to Zn^{II} was investigated by probing the reaction of acetate and the model complexes by ^1H NMR in DMSO-d_6. The water content was decreased as much as possible to avoid hydrolysis of the substrate. Acetate ion, was chosen as a model to evaluate the influence of coordination sphere in the coordination of carboxylate and its polarization by the metal. In addition, the chemical shifts would allow to indirectly evaluate the Lewis acidity. The comparative spectra are showed in the ESI (Fig. S3†) and the respective methyl chemical shifts reported in the Table 4.

The methyl hydrogens of acetate were deshielded when added to the solution of the Zn^{II} complexes. The deshielding observed is consistent with the coordination of the carboxylate to the metal ion and dependent on the coordination sphere of the Zn^{II} complex. The extension of the shift in the methyl signals, ($\Delta\delta$) reflects the charge donation of the carboxylate to the metal, which can be indirectly associated with the electronic density (or alternatively, the acidity) of the metal ion.

Our results showed that the presence of a soft donor sulfur atom bound to the zinc strongly affected the acetate coordinated suggesting a higher electron density over Zn^{II} decreasing the acetate coordination to the complex [Zn(N-NNS)], similarly to the Zn^{II} added in the form of nitrate salt. The exchange of Cl^- in [Zn(N-NNS)] by solvent molecules is observed by NMR (Fig. S6B†). On the other hand, the presence of the oxygen base or the nitrogen donor causes a decrease in the electronic density over Zn^{II}, favoring acetate coordination.

Previous studies concerning Zn^{II} hydrolytic metalloenzymes showed the importance of this carboxylate coordination for reactivity.[17,27,74] The hydrolytic kinetics of β-lactams is affected by the extension of the polarization of the carboxylate bond due to the coordination to zinc. The NMR study suggests [Zn(N-NNO)] induces the strongest polarization of the carboxylate bond whereas the [Zn(N-NNS)] the lowest, and agreeing with previously kinetic rate order: [Zn(N-NNO)] > [Zn(N-NNN)] > [Zn(N-NNS)].

A similar experiment was performed using the broadly used in clinic penam, amoxicillin. The complexes were mixed with equivalent amounts of amoxicillin and ^1H NMR spectrum was acquired. Fig. 5 shows the hydrogen probed in the amoxicillin structure.[22,74] The ^1H NMR spectra of the resulting mixtures indicate the coordination of amoxicillin to the complexes (see ESI Fig. S4†). The probe signals are highlighted and its chemical shift is reported in Table 4 for each Zn complex. The shift in the signal of the geminal hydrogen to the carboxylate compared to the free amoxicillin spectrum suggests that the coordination occurs *via* carboxylate towards the Zn^{II}. This behavior is consistent with expected for MβL models, in which the first hydrolysis step is the substrate coordination and fundamental to the subsequent reactions.

The chemical shift changes ($\Delta\delta$) observed upon coordination with amoxicillin evidence [Zn(N-NNO)] is the most polarizing, followed by [Zn(N-NNN)] and then [Zn(N-NNS)]. For the first two complexes, the $\Delta\delta$ of the geminal hydrogen was positive and consistent with the deshielding upon coordination. For the [Zn(N-NNS)], the $\Delta\delta$ was negative suggesting that a secondary interaction is taking place. More than one Zn^{II} complex might be interacting with one molecule of amoxicillin. The shifting and broadening of the amoxicillin signals at around 1.5 ppm by the mixture with [Zn(N-NNS)] can indicate some secondary interaction. ITC data are going to corroborate to this hypothesis and will be discussed in the section 3.5. In general, all complexes [Zn(N-NNX)], with X = O, N or S, showed to interact with amoxicillin *via* coordination of the carboxylate and following the previously found polarization order of the Zn^{II} in the model complexes. The $Zn(NO_3)_2$ caused the highest shift in this case showing strong interaction with the carboxylate. In the ^1H spectra of the amoxicillin with Zn^{II} complexes, the ligand hydrogens signals were also evaluated. For both [Zn(N-NNN)] and [Zn(N-NNS)] no significant change in the tripodal ligand chemical shifts was observed, allowing no further conclusion. Both spectra are shown in ESI Fig. S5 and S6† repectively.

The spectral changes in the tripodal ligand of [Zn(N-NNO)] upon addition of amoxicillin, ESI Fig. S7,† involved changes in the coupling pattern and in the chemical shift variation ($\Delta\delta$), that are displayed in Table 5 with the respectively assigned structure shown in Fig. 6. Knowing that before amoxicillin coordination [Zn(N-NNO)] have an octahedral geometry,

Table 4 ^1H NMR evaluation of the complex interaction with carboxylate following the signals in the methyl moiety in potassium acetate or carboxylate geminal hydrogen H_{probe} (Fig. 5) in amoxicillin as electronic probes in DMSO-d_6

	KOAc		Amoxicillin	
Compound	δ (ppm)	$\Delta\delta$ (ppm)	δ (ppm)	$\Delta\delta$ (ppm)
Probe + [Zn(N-NNO)]	2.00	+0.43	4.76	+0.09
Probe + [Zn(N-NNN)]	1.98	+0.41	4.74	+0.07
Probe + [Zn(N-NNS)]	1.74	+0.17	4.48	−0.19
Probe + $Zn(NO_3)_2$	1.74	+0.17	4.90	+0.23
Probe	1.57	0	4.67	0

Table 5 [Zn(N-NNO)] ligand ^{1}H NMR evaluation upon coordination with amoxicillin in d_6-DMSO. The δ corresponds to the chemical shift of the hydrogen after the interaction, and $\Delta\delta$ corresponds to the variation using the signal of the original complexes in d_6-DMSO

Hydrogen	δ (ppm)	$\Delta\delta$ (ppm)	Multiplicity
H_1	8.90	+0.24	D
H_5	4.29	+0.06	S
H_6	3.13	−0.12	S

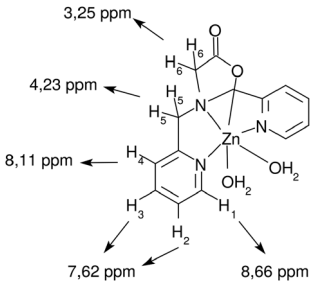

Fig. 6 Molecular structure of the [Zn(N-NNO)] complex with numbered atoms and ^{1}H NMR chemical shifts obtained in DMSO-d_6.

favored by the water coordinated instead of chloride, the coordination of a more hindered ligand, as amoxicillin, should lead to a lower coordination number and changing the overall complex geometry. In spite of the amoxicillin signal appearance, changes in the chemical shift of the H_1 and, in the coupling pattern of the H_5 signal, were observed. The largest changes in the ligand signals were the H_1 in the pyridines *ortho* to the nitrogen bonded to the zinc, and the benzylic hydrogen atoms, neighbors to the tertiary amine. The coordination of amoxicillin leads to a change in the complex structure that is seen by the change in the coupling pattern (H_5). In the free complex, the H_5 signal is a doublet of doublets (AB quartet) and after the interaction, it collapses to a singlet. Such singlet appearance indicates a change in the complex structure and gain of symmetry, that leads to a chemical and magnetic equivalence of these hydrogens. This suggests a change in the zinc coordination sphere upon amoxicillin binding.

To theoretically evaluate the zinc electronic density and reactivity, DFT was used to obtain Fukui indices. Recently, DFT has been successfully applied in the study of organic molecules and metal complexes, providing relevant insight into their reactivity.[76–79] More specifically, global reactivity parameters such as electronegativity, hardness and electrophilicity indices, as well as local indices as local softness and the Fukui functions are capable of being obtained by such approach.[80–84]

The Fukui indices represent an important tool to give a local insight of reactivity site. It measures how sensitive a chemical system is to an external perturbation at a particular point. It provides the same information as the local softness and can be used instead. The perturbation can be the addition of electrons (f^+) or removal of electrons (f^-). The partial charge presented in the Fukui functions is obtained from a population analysis. A few schemes for population analysis are described, as Natural Bond Orbitals, Mulliken and Hirshfeld analysis.[59,85,86] Roy *et al.*[85] have shown the latter is more reliable for calculating local reactivity descriptors and also produces non-negative condensed Fukui functions.[86] Even with the fact that negative Fukui index values are considered as an acceptable orbital relaxation effect,[59,87] for this work all the comparison were made using only positive Fukui indices.

We calculated Fukui indices for the complexes [Zn(N-NNO)], [Zn(N-NNN)], and [Zn(N-NNS)] using two different functionals (PBE and PBE0)[88] and two population analysis (Hirshfeld – HSA and Natural – NPA).[89,90] The results obtained using PBE or PBE0 and HSA showed only positive indexes for the zinc atom and the same trend between the analyzed complexes, thus the PBE0/HSA was selected for further discussion.[85,86] For NPA, some negative indexes were found. Considering these negative indexes as consequence of orbital relaxation effect,[59,87] a similar trend was observed. Fukui indexes for Zn atoms using PBE0/HSA are reported in Table 6. The complete table of results is reported on the ESI (Tables S2–S5†), which shows the Fukui index values (f^+ & f^-) split into PBE and PBE0 and using the numbering scheme showed in Fig. 4. A significant difference in Fukui indexes of Zn atom in the complexes was obtained. The following order was found for the susceptibility for the Zn^{II} ions receive electrons [Zn(N-NNO)] > [Zn(N-NNN)] > [Zn(N-NNS)] as demonstrated by the values of f^+. It suggests the presence of nitrogen and sulfur in the coordination sphere lead to a lower electrophilicity of the metal, corroborating the previous findings.

3.4. X-ray absorption spectroscopy

To investigate the influence of the coordination sphere on the zinc electronic density, X-ray absorption spectroscopy (XAS) experiments were performed. XAS stands out due to its element-specificity, as well as high sensitivity towards both electronic and geometric structures around the atom.[91–96] The Zn K-edge XAS analysis was focused on the near-edge region (also referred to as XANES – X-ray absorption near edge spectroscopy), as when combined to quantum chemical calculations, it is able to provide detailed information on the electronic density over the metal center of molecules.[55,96,97] Such information is essential to evaluate the hypothesis that the electronic density around the zinc in the model compounds studied here is influenced by coordination sphere and also influences the reactivity. The individual XAS spectra of all three complexes are presented in Fig. S8–S10 in the ESI.† The normalized XANES spectra are shown in Fig. 7.

Table 6 Zn^{II} fukui index values (f^+ & f^-) for Hirshfeld Population Analysis (HPA) by employing the PBE0 functional

Complex	f^+	f^-
[Zn(NNO)]	0.015665	0.024586
[Zn(NNN)]	0.006815	0.040195
[Zn(NNS)]	0.003795	0.051891

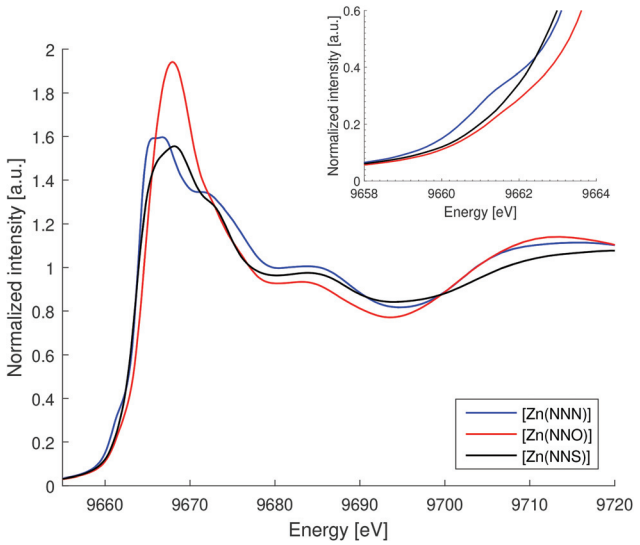

Fig. 7 Zn K-edge X-ray absorption spectra of solid model complexes [Zn(N-NNX)], with X = O, N or S. Insert showing pre-edge absorptions observed for the complexes.

The overall electronic density around the Zn atom can be directly correlated with the Zn K-edge rising edge energies ($E_{\text{K-edge}}$) of the complexes.[94,97,98] The $E_{\text{K-edge}}$ was taken as the maximum of the first derivative of the edge, being: 9663.0; 9663.5 and 9664.3 eV for [Zn(N-NNS)], [Zn(N-NNN)] and [Zn(N-NNO)] respectively, as shown in Fig. S11.† A trend in the edge position as a function of coordination environment is then observed. An increasing value of $E_{\text{K-edge}}$ was observed, following the order [Zn(N-NNS)] < [Zn(N-NNN)] < [Zn(N-NNO)]. Such order indicates that the [Zn(N-NNO)] model has the lowest effective electronic density zinc atom and the [Zn(N-NNS)] has the highest, supporting the hypothesis previously raised. This is a final evidence, now directly probed in the metal center, that the coordination sphere modulates the metal electronic density and affects directly the hydrolytic β-lactam activity of these Zn^{II} MβL models.

Furthermore, unexpected pre-edge features were observed for the [Zn(N-NNN)] and [Zn(N-NNO)] complexes, as evidenced in the insert in Fig. 7. These absorptions are related to inner-orbital electrons (1s for the K-edge) to the empty valence shell, being commonly observed for transition metals with mixed unoccupied p and d-orbitals like Mn, Fe or Co.[57,99–101] The presence of these weak transitions is rather unusual in Zn complexes,[102,103] and we employed a well-established TDDFT methodology to provide further insight in their origins.[55,104,105] The most pronounced pre-edge absorption is observed for the [Zn(N-NNN)] complex centered at about 9660.0 eV. In the case of [Zn(N-NNO)], only a subtle shoulder can be observed in the spectrum, which is more clearly noticed by investigating the first derivative (Fig. S11†) observed near 9661.2 eV. The [Zn(N-NNS)] did not show any clear pre-edge feature. The pre-edge absorption energies can be found in Table S7.†

TDDFT has been successfully applied in describing pre-edge features of metal complexes, rationalizing the origins of the transitions underlying such features, and at the same time, providing detailed information about the electronic structure.[55,97,98] For [Zn(N-NNN)] and [Zn(N-NNS)], only DFT optimized structures were used due to the high structural similarity between the crystal and optimized structures. For [Zn(N-NNO)], the DFT optimized structure obtained had a small but significant difference from the crystalline one, that showed to affect the simulated spectrum. Thus, a bipyramid geometry with chloride coordinated in the place of water was calculated in order to evaluate the effect of these structural changes in the simulated spectrum. Thereby, the crystal structure (Fig. 8a), a distorted octahedral optimized (Fig. 8b) and a trigonal bipyramidal model ((Fig. 8c, with chloride coordinated) of [Zn(N-NNO)] were evaluated and will be discussed. A comparison of the experimental and calculated pre-edge regions, with applied energy shift of +93.5 eV, is shown in Fig. 9.

The TDDFT-calculated pre-edges follow the same trend observed experimentally, predicting pre-edge absorptions for [Zn(N-NNN)] and [Zn(N-NNO)] complexes, as well as a much less pronounced feature in the spectrum of [Zn(N-NNS)]. The Kohn–Sham orbitals assigned to these transitions of [Zn(N-NNS)], [Zn(N-NNO)] (crystal structure) and [Zn(N-NNS)] are shown in Fig. 10. The spectra with the molecular orbitals assigned to pre-edge transitions are shown in Fig. S12–S14.† The [Zn(N-NNN)] pre-edge feature is a metal-to-ligand charge transfer (MLCT) excitation into low lying pyridine π* orbitals. [Zn(N-NNS)] and [Zn(N-NNO)] have MLCT transitions into pyridine π* orbitals of similar energy, but they are barely visible in their spectra. This transitions to π* states are shown in Fig. 10 and in agreement with previous results observed for manganese complexes with pyridine-rich ligands.[97]

The crystal structure of [Zn(N-NNO)] is octahedral with two H_2O molecules coordinated to it, whereas the other complexes

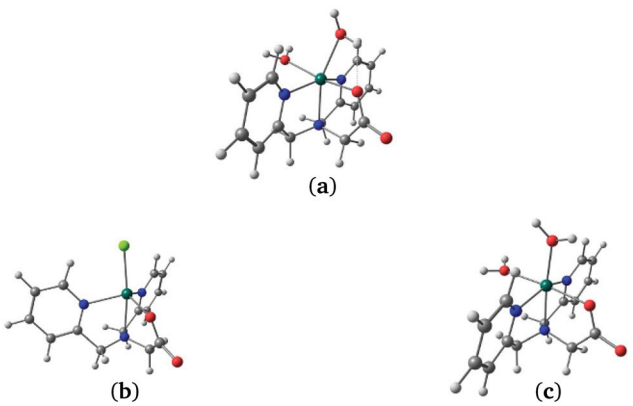

Fig. 8 Structures of [Zn(N-NNO)] used for the Zn K-edge pre-edge absorption calculations. The coordination sphere geometry and octahedral distortion due to the coordinated water were evaluated using (a) DFT octahedral and (b) model trigonal bipyramid and (c) crystal structures. Nitrogen atoms are colored in blue, oxygen in red, carbon in grey, zinc in dark green and chlorine atoms in light green.

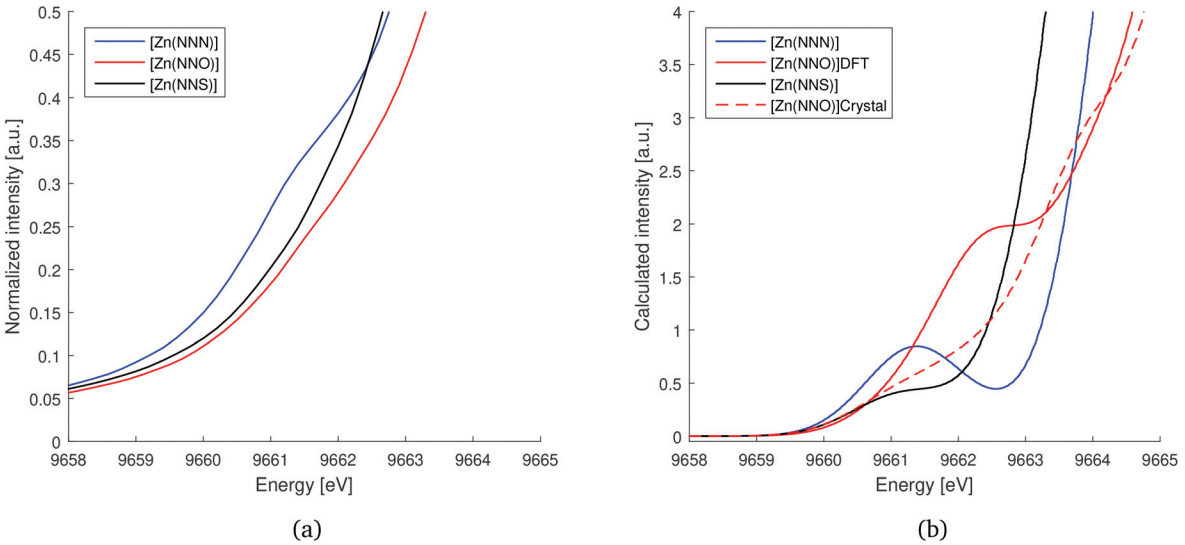

Fig. 9 Comparative Zn K-edge X-ray absorption spectra of (a) experimental solid complexes [Zn(N-NNX)], with X = O, N or S, and (b) TDDFT calculated pre-edge absorptions using the optimized structures, including a calculation using the crystal structure of [Zn(N-NNO)].

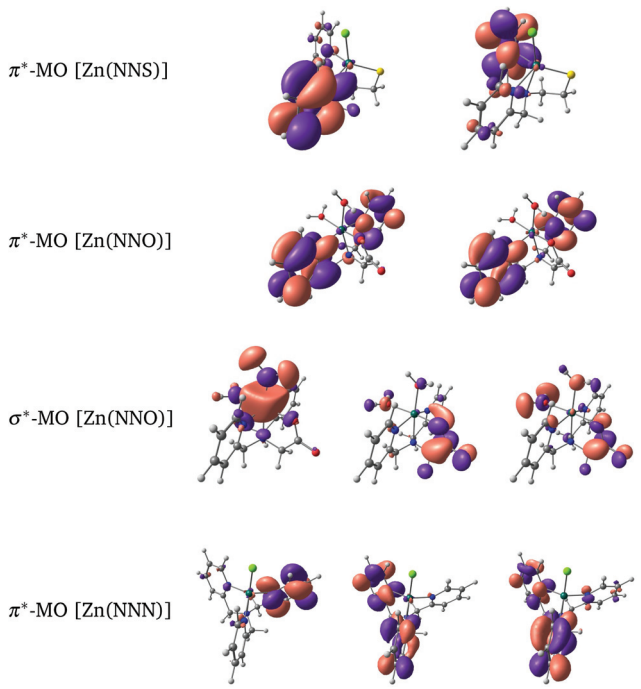

Fig. 10 TDDFT calculated Kohn–Sham molecular orbitals (MO) involved in state transitions assigned to experimentally observed K-edge pre-edge absorptions for [Zn(N-NNS)], [Zn(N-NNN)] and [Zn(N-NNO)] complexes. For [Zn(N-NNO)], both σ* and π* orbitals were observed, but for [Zn(N-NNN)] and [Zn(N-NNS)] only π* orbitals were obtained. Nitrogen atoms are colored in blue, oxygen in red, carbon in grey, sulfur in yellow, zinc in dark green and chlorine atoms in light green.

assume a distorted trigonal bipyramidal geometry with a single chloride ligand in the axial position. Thus, a hypothetical trigonal bipyramidal [Zn(N-NNO)] was calculated using chlorine coordinated, instead of water, in order to evaluate the effect of the coordination sphere geometry over the π* orbitals energy. These calculations showed that the π* orbitals states have lower energy in the trigonal bipyramidal geometry complexes than [Zn(N-NNO)] complex in an octahedral geometry. Therefore, leading to a pre-edge absorption with lower energy for a hypothetical trigonal bipyramidal complex.

Furthermore, these TDDFT calculations for [Zn(N-NNO)] showed a significant change in the spectrum depending on the angular distortion of the coordinated water. Thereby, crystal (Fig. 8a) and DFT optimized (Fig. 8b) were used for the TDDFT calculation and showed that the crystal packing has an important effect over the position and angles of the Zn^{II} coordinated water molecules that directly affects the TDDFT absorptions energy. The pre-edge absorptions observed for the [Zn(N-NNO)] octahedral complex is twofold, involving π* and σ* states in its composition. The transition to σ* state involves Zn s and p orbitals mixed with water oxygen orbitals, shown in Fig. 10, and this contribution has a lowered energy when compared with the transition to π* states. This σ*-transition showed to be highly dependent on the structure used in the calculation and gaining intensity when the DFT optimized structure was used (see Fig. 9). In the [Zn(N-NNO)] DFT structure (Fig. 8b), the absence of the packing effect lead to distortion induced that decreases the σ* orbitals energy. Thus, leading to a lower energy for this transition in this DFT structure than for the crystal structure. This is also followed by a gain in intensity for the DFT structure compared to the crystal one. Thus, the TDDFT calculation for [Zn(N-NNO)] crystal structure agrees with the experimental spectrum obtained for this complex.

3.5. Thermodynamic parameters of [Zn(N-NNX)] and amoxicillin reaction

The formation of the enzyme–substrate complex is a determinant step for enzymatic reactions. In the case of monozinc

MβL the most accepted mechanism is the coordination of one molecule of β-lactam compound per active site by the carboxylate group closest to the β-lactam ring followed by the water attack.[1,2,27,74] The formation of [Zn(amox)] complex is very difficult to be detected and mimetic compounds have been used to structurally determine it.[22,23] Therefore, the thermodynamic measurement of this enzyme–substrate adduct formation can be performed in order to evaluate the affinity and mechanism without a structural analysis.[106,107]

Isothermal titration calorimetry (ITC) is a sensitive technique to determine affinity constants, the stoichiometric ratio between enzyme models and the substrate, and thermodynamic parameters as ΔG, ΔH and $T\Delta S$.[108] In this work ITC was used to evaluate the effect of the first coordination sphere of the complex in the coordination with amoxicillin (the model substrate). The measurement was performed in dried DMSO in order to avoid hydrolysis of the β-lactam. The ITC data are summarized in Table 7. All enthalpy variation plots are presented as Fig. S15–S17 in the ESI.†

The data show a thermodynamically favorable interaction for all the complexes ($\Delta G < 0$). The stoichiometry relation between amoxicillin and the complexes changes dramatically depending on the ligand, showing an important effect of the Zn^{II} coordination sphere on the behavior of the formed system in equilibrium. It is important to highlight that ligand exchange reaction of the complex and the solvent were corrected by measuring blank solutions in the sample cell. The dilution heat of amoxicillin was also corrected. The heat measured corresponds to the interaction of the amoxicillin and the complex. It is possible to see that for [Zn(N-NNS)] the stoichiometry relation is the lowest, suggesting a system arrangement with 3 : 1 complex : amoxicillin ratio. Such arrangement supports the hypothesis of secondary interactions of the amoxicillin with the complexes rather than the carboxylate coordination only, as suggested by the negative shift in the ^{1}H NMR interaction experiment (see Table 4). For [Zn(N-NNO)], a 1 : 1 complex : amoxicillin ratio was observed, agreeing with the expected for a simple coordination, but for [Zn(N-NNN)], a 2 : 1 complex : amoxicillin ratio was obtained, suggesting more than one complex is interacting with one molecule of amoxicillin (multiple interactions). This ratio should be further studied using techniques to evaluate the species in equilibrium for each complex. The ITC data allow to say that the thiolate coordination is facilitating the ligand exchange and multiple interactions, followed by [Zn(N-NNN)] and the well behaved [Zn(N-NNO)]. The trend corroborates previous results, however charge effects cannot be disregarded. The multiple interactions revealed by the ITC data must contribute to the hydrolysis kinetics. Taken the numbers of k_{obs} measured (Table 3) the secondary interactions does not turn the complex more active than the [Zn(N-NNO)] which presented a stoichiometric ratio 1 : 1. It is not possible to conclude with the data if it is cooperative or non-cooperative interaction. The NMR data suggests interaction of [Zn(N-NNS)] and thioether bond of amoxicillin, but it is not confident. Multiple interactions were reported for the reaction of 8-hydroxyquinoline and Zn^{II} complex with tripodal ligands, and also in dinuclear models.[75,108]

Table 7 Thermodynamic data obtained by ITC of [Zn(N-NNX)], X = S, N or O, complexes with amoxicillin in dry DMSO at 25 °C

	[Zn(N-NNS)]	[Zn(N-NNN)]	[Zn(N-NNO)]
N	0.34	0.54	1.04
K	6.9×10^5	2.9×10^5	9.2×10^3
ΔH (kJ mol^{-1})	−51.0	−51.6	−21.6
ΔS (J mol^{-1} K^{-1})	−59	−68	+3
$-T\Delta S$ (kJ mol^{-1})	17.7	20.5	−1.0
ΔG (kJ mol^{-1})	−33.3	−31.1	−22.6

The equilibrium constants are similar for [Zn(N-NNS)] and [Zn(N-NNN)], being two orders of magnitude smaller for [Zn(N-NNO)]. Enthalpy variation changes are all negative and for [Zn(N-NNS)] and [Zn(N-NNN)] they are very similar, however, in the case of [Zn(N-NNO)], it is less than half of that of the other compounds. Thereby, suggesting an important change in the Zn^{II} reactivity in the presence of the carboxylate moiety.

[ZnZn] was also measured using the same procedures but showed a low equilibrium constant that did not allow fitting for quantitative analysis (see ESI Fig. S18†).[65] Our results point out that the ligand choice for the synthetic MβL zinc model is an important factor to control its reactivity. Thus, the ligand choice should be made with care in order to allow a correct understanding of the enzymatic mechanism and an investigation of potential inhibitors.[108]

4. Conclusion

Understanding the influence of the coordination sphere over MβL reactivity is a relevant topic to allow the development of new inhibitors and antimicrobial compounds. We studied it using a series of zinc complexes that were synthesized aiming to better model coordination structures of MβL active sites. These complexes had their structures and reactivity evaluated using XRD, nitrocefin hydrolysis kinetics, ^{1}H NMR, Zn K-edge XAS and ITC with the purpose of understanding how changes in the coordination sphere would change the reactivity towards β-lactam hydrolysis. We observed that changes in the ligands in order to increase its electronic donation toward the zinc atom decreases the ability of the complex to hydrolyse β-lactam compounds, which can be explained by the lower electrophilicity (overall higher electronic density) of zinc, its strength to coordinate the substrate and favor the water (or hydroxide) attack.

Model complexes of MβL have been successfully used for the understanding of the mechanism of β-lactam hydrolysis.[2,22,23] However, in the previous work not much attention was devoted to the Zn^{II} Lewis acidity in these systems considering the differences among MβL subclasses (B1, B2, and B3). The classification reveals that the sequence of coordinating amino acids also changes the reactivity.[1] This work represents

the first systematic study of the influence of pyridine, thiolate and carboxylate groups over the electronic density (Lewis acidity) of Zn^{II} ions in MβL model complexes and the corresponding effect on reactivity.

X-ray absorption near edge structure (XANES) spectra of the model complexes were fundamental to show the overall metal electronic density, demonstrating that the Lewis acidity of Zn^{II} ions is strongly influenced by donor groups. Thiolate is the strongest donor and consequently [Zn(N-NNS)] is the weakest acid, oppositely by the carboxylate donor in the [Zn(N-NNO)] complex. The presence of pyridine donor groups generates low lying anti-bonding orbitals, indicated by the presence of weak pre-edge features in the zinc K-edge XAS spectra.[97] They are also highly influenced by the third donor arm in the tripodal system. TDDFT was able to predict the transitions for all tripodal complexes. In the case of [Zn(N-NNO)], the geometry of coordinating waters was shown to influence the pre-edge transitions. The observed difference in the Lewis acidity influences directly the hydrolysis kinetics of the complexes, which follows the same order found for the Zn K-edge energies ([Zn(N-NNS)] < [Zn(N-NNN)] < [Zn(N-NNO)]).

The mechanism of hydrolysis for these complexes was revealed by NMR studies. It consists of the carboxylate (closest to the β-lactam ring) coordination to the metal, facilitating the nucleophilic attack, in agreement with other MβL model compounds.[22] It is highly influenced by the Lewis acidity, and [Zn(N-NNS)] is less polarizing than [Zn(N-NNO)] as demonstrated by the NMR study using acetate as the probe. The NMR study using amoxicillin as the probe demonstrates that [Zn(N-NNS)] is subjected to secondary interactions and the isothermal titration calorimetry (ITC) revealed a stoichiometry of 1 : 3 amoxicillin : complexes ratio, confirming the interactions with groups other than the carboxylate. Besides the ligand effect on the Lewis acidity, the hard/soft character is also affected. The results indicate that the thiolate softens the metal center and favors the interaction with amines, amides or thioether groups present in amoxicillin, in addition to DMSO or solvents with soft character. The Pearson theory is better to explain why [Zn(N-NNS)] presents a facilitated exchange with DMSO in comparison with [Zn(N-NNO)] and also presents a stoichiometry that indicates these multiple interactions with amoxicillin. The [Zn(N-NNN)] presented 1 : 2 amoxicillin : complex ratio also revealing secondary interactions, while [Zn(N-NNO)] showed 1 : 1 ratio. These results show that the softer the metal center, more favorable are the secondary interactions. In the enzymatic system, the whole protein directs the substrate avoiding the unwanted interactions. The ITC results for the interaction with amoxicillin revealed enthalpies following the order [Zn(N-NNS)] ~ [Zn(N-NNN)] ≫ [Zn(N-NNO)]. The higher enthalpies for [Zn(N-NNN)] and [Zn(N-NNS)] are a result of the presence of other bonds besides the carboxylate coordination.

Geometrically the complexes revealed important differences in bond lengths and angles among themselves. The presence of the carboxylate donor group in [Zn(N-NNO)] favors the octahedral geometry, while trigonal bipyramidal was found for [Zn(N-NNN)] and [Zn(N-NNS)]. However, compared to the [ZnZn], the tripodal complexes shared more similarities to the GOB 5K0W enzyme active site than the dinuclear model.[71]

In summary, the work demonstrated that the Zn^{II} acidity cannot be disregarded in the design of MβL model compounds, as it influences the reactivity and kinetics. Also, it reveals that the presence of thiolate ligands softens the zinc center and similar behavior might be found in the enzymes B1 and B2 (Asp, Cys, His) in contrast to B3 (His, His, Asp). This is a relevant point of MβL diversity that makes the inhibitor design a challenge. Besides their similar active site structures, several aspects differ among the subclasses and specific inhibitors must be developed.

Conflicts of interest

There are no conflicts to declare.

Acknowledgements

This work was supported by São Paulo Research Foundation (FAPESP Grant number 2017/127190), Brazilian National Council for Scientific and Technological Development (CNPq Grant number 140367/2015-2), and the Foundation for Research and Extension of the University of Campinas (FAEPEX Grant number 519.292-1 Aux. 145/16). This study was financed in part by the Coordenação de Aperfeiçoamento de Pessoal de Nível Superior – Brasil (CAPES) – Finance Code 001. This research used resources of the Brazilian Synchrotron Light Laboratory (LNLS), an open national facility operated by the Brazilian Center for Research in Energy and Materials (CNPEM) for the Brazilian Ministry for Science, Technology, Innovations and Communications (MCTIC), proposals 20170190 and 20171108. The XAFS1 and XAFS2 beamline staff is acknowledged for the assistance during the experiments. The authors would like to thank Maria das Graças de Oliveira e Silva, Catherine Moraes Teles, Carolina Galuppo, Letícia Graziele Ferraresso, Tainá Prazeres Leal de Moraes e Raphael Honorato Ribeiro for the help with experimental measurements and suggestions and Fernando R. G. Bergamini for the cover artwork.

References

1 A. I. Karsisiotis, C. F. Damblon and G. C. K. Roberts, *Metallomics*, 2014, **6**, 1181–1197.
2 L. J. Daumann, G. Schenk and L. R. Gahan, *Eur. J. Inorg. Chem.*, 2014, **2014**, 2869–2885.
3 WHO, *Antimicrobial resistance: global report on surveillance*, World Health Organization, 2014.
4 D. T. King and N. C. Strynadka, *Future Med. Chem.*, 2013, **5**, 1243–1263.
5 H. A. Kirst, *Expert Opin. Pharmacother.*, 2015, **16**, 149–150.
6 E. E. Gill, O. L. Franco and R. E. W. Hancock, *Chem. Biol. Drug Des.*, 2015, **85**, 56–78.

7 C. d. M. Bertoncheli and R. Horner, *Braz. J. Pharm. Sci*, 2008, **44**, 577–599.
8 J. Chen, X. Shang, F. Hu, X. Lao, X. Gao, H. Zheng and W. Yao, *Mini-Rev. Med. Chem.*, 2013, **13**, 1846–1861.
9 X.-L. Liu, Y. Shi, J. S. Kang, P. Oelschlaeger and K.-W. Yang, *ACS Med. Chem. Lett.*, 2015, **6**, 660–664.
10 Y. Hiraiwa, A. Morinaka, T. Fukushima and T. Kudo, *Bioorg. Med. Chem.*, 2013, **21**, 5841–5850.
11 J.-I. Wachino, Y. Yamaguchi, S. Mori, H. Kurosaki, Y. Arakawa and K. Shibayama, *Antimicrob. Agents Chemother.*, 2013, **57**, 101–109.
12 M. S. Mohamed, W. M. Hussein, R. P. McGeary, P. Vella, G. Schenk and R. H. Abd El-hameed, *Eur. J. Med. Chem.*, 2011, **46**, 6075–6082.
13 A. M. Somboro, D. Tiwari, L. A. Bester, R. Parboosing, L. Chonco, H. G. Kruger, P. I. Arvidsson, T. Govender, T. Naicker and S. Y. Essack, *J. Antimicrob. Chemother.*, 2015, **70**, 1594–1596.
14 G. Parkin, *Chem. Rev.*, 2004, **104**, 699–768.
15 Y. Valasatava, A. Rosato, N. Furnham, J. M. Thornton and C. Andreini, *J. Inorg. Biochem.*, 2018, **179**, 40–53.
16 M. Laitaoja, J. Valjakka and J. Janis, *Inorg. Chem.*, 2013, **52**, 10983–10991.
17 M. L. Zastrow and V. L. Pecoraro, *Biochemistry*, 2014, **53**, 957–978.
18 N. O. Concha, B. A. Rasmussen, K. Bush and O. Herzberg, *Structure*, 1996, **4**, 823–836.
19 G. Garau, C. Bebrone, C. Anne, M. Galleni, J.-M. Frère and O. Dideberg, *J. Mol. Biol.*, 2005, **345**, 785–795.
20 J. Ullah, T. Walsh, I. Taylor, D. Emery, C. Verma, S. Gamblin and J. Spencer, *J. Mol. Biol.*, 1998, **284**, 125–136.
21 J. M. González, M.-R. Meini, P. E. Tomatis, F. J. M. Martín, J. A. Cricco and A. J. Vila, *Nat. Chem. Biol.*, 2012, **8**, 698–700.
22 N. V. Kaminskaia, B. Spingler and S. J. Lippard, *J. Am. Chem. Soc.*, 2000, **122**, 6411–6422.
23 N. V. Kaminskaia, B. Spingler and S. J. Lippard, *J. Am. Chem. Soc.*, 2001, **123**, 6555–6563.
24 N. Burzlaff, *Concepts and Models in Bioinorganic Chemistry - 17 Model Complexes for Zinc-Containing Enzymes*, Wiley-VCH, 1st edn, 2006.
25 Z. Wang, W. Fast and S. J. Benkovic, *Biochemistry*, 1999, **38**, 10013–10023.
26 N. Díaz, D. Suárez and K. M. Merz, *J. Am. Chem. Soc.*, 2000, **122**, 4197–4208.
27 M.-N. Lisa, A. R. Palacios, M. Aitha, M. M. González, D. M. Moreno, M. W. Crowder, R. A. Bonomo, J. Spencer, D. L. Tierney, L. I. Llarrull and A. J. Vila, *Nat. Commun.*, 2017, **8**, 538–549.
28 H. Zhang and Q. Hao, *FASEB J.*, 2011, **25**, 2574–2582.
29 W. L. Armarego and C. Chai, *Purification of Laboratory Chemicals*, 7th edn, Butterworth-Heinemann, Boston, 2013, pp. 103–554.
30 B. Xu, W. Zhong, Z. Wei, H. Wang, J. Liu, L. Wu, Y. Feng and X. Liu, *Dalton Trans.*, 2014, **43**, 15337–15345.
31 Y. Liu, R. Xiang, X. Du, Y. Ding and B. Ma, *Chem. Commun.*, 2014, **50**, 12779–12782.
32 N. Lazarova, J. Babich, J. Valliant, P. Schaffer, S. James and J. Zubieta, *Inorg. Chem.*, 2005, **44**, 6763–6770.
33 H. Kurosaki, T. Tawada, S. Kawasoe, Y. Ohashi and M. Goto, *Bioorg. Med. Chem. Lett.*, 2000, **10**, 1333–1337.
34 A. Abufarag and H. Vahrenkamp, *Inorg. Chem.*, 1995, **34**, 2207–2216.
35 G. R. Fulmer, A. J. M. Miller, N. H. Sherden, H. E. Gottlieb, A. Nudelman, B. M. Stoltz, J. E. Bercaw and K. I. Goldberg, *Organometallics*, 2010, **29**, 2176–2179.
36 G. M. Sheldrick, *Acta Crystallogr., Sect. A: Found. Crystallogr.*, 2008, **64**, 112–122.
37 A. L. Spek, *J. Appl. Crystallogr.*, 2003, **36**, 7–13.
38 J.-P. Bégué, D. Bonnet-Delpon and B. Crousse, *Synlett*, 2004, 18–29.
39 M. Tajbakhsh, R. Hosseinzadeh, H. Alinezhad, S. Ghahari, A. Heydari and S. Khaksar, *Synthesis*, 2011, 490–496.
40 W. Xu, J. A. Craft, P. R. Fontenot, M. Barens, K. D. Knierim, J. H. Albering, F. A. Mautner and S. S. Massoud, *Inorg. Chim. Acta*, 2011, **373**, 159–166.
41 B. Ravel and M. Newville, *J. Synchrotron Radiat.*, 2005, **12**, 537–541.
42 H. C. N. Tolentino, A. Y. Ramos, M. C. M. Alves, R. A. Barrea, E. Tamura, J. C. Cezar and N. Watanabe, *J. Synchrotron Radiat.*, 2001, **8**, 1040–1046.
43 S. J. A. Figueroa, J. C. Mauricio, J. Murari, D. B. Beniz, J. R. Piton, H. H. Slepicka, M. F. de Sousa, A. M. Espíndola and A. P. S. Levinsky, *J. Phys. Conf. Ser.*, 2016, **712**, 012022.
44 F. Neese, *Wiley Interdiscip. Rev.: Comput. Mol. Sci.*, 2017, **2**, 73–78.
45 F. Weigend and R. Ahlrichs, *Phys. Chem. Chem. Phys.*, 2005, **7**, 3297–3305.
46 Schrödinger, LLC, *The PyMOL Molecular Graphics System, Version 1.7.2.1*, 2015.
47 T. Petrenko, S. Kossmann and F. Neese, *J. Chem. Phys.*, 2011, **134**, 1–14.
48 R. Izsák and F. Neese, *J. Chem. Phys.*, 2011, **135**, 1–11.
49 F. Neese, F. Wennmohs, A. Hansen and U. Becker, *Chem. Phys.*, 2009, **356**, 98–109.
50 G. Jansen and B. A. Hess, *Phys. Rev. A*, 1989, **39**, 6016–6017.
51 R. Samzow, B. A. Hess and G. Jansen, *J. Chem. Phys.*, 1992, **96**, 1227–1231.
52 D. A. Pantazis, X.-Y. Chen, C. R. Landis and F. Neese, *J. Chem. Theory Comput.*, 2008, **4**, 908–919.
53 M. Cossi, N. Rega, G. Scalmani and V. Barone, *J. Comput. Chem.*, 2003, **24**, 669–681.
54 M. O. Krause and J. Oliver, *J. Phys. Chem. Ref. Data*, 1979, **8**, 329–338.
55 S. DeBeer George, T. Petrenko and F. Neese, *J. Phys. Chem. A*, 2008, **112**, 12936–12943.
56 P. Chandrasekaran, S. C. E. Stieber, T. J. Collins, L. Que Jr., F. Neese and S. DeBeer, *Dalton Trans.*, 2011, **40**, 11070–11079.

57 J. A. Rees, R. Bjornsson, J. K. Kowalska, F. A. Lima, J. Schlesier, D. Sippel, T. Weyhermuller, O. Einsle, J. A. Kovacs and S. DeBeer, *Dalton Trans.*, 2017, **46**, 2445–2455.
58 P. W. Ayers, F. D. Proft, A. Borgoo and P. Geerlings, *J. Chem. Phys.*, 2007, **126**, 2544–2551.
59 P. W. Ayers, F. D. Proft, A. Borgoo and P. Geerlings, *J. Chem. Phys.*, 2007, **126**, 224107.
60 S. Grimme, J. Antony, S. Ehrlich and H. Krieg, *J. Chem. Phys.*, 2010, **132**, 154104.
61 F. L. Hirshfeld, *Theor. Chem. Acc.*, 1977, **44**, 129–138.
62 A. E. Reed, R. B. Weinstock and F. Weinhold, *J. Chem. Phys.*, 1985, **83**, 735–746.
63 T. Y. Nikolaienko, L. A. Bulavin and D. M. Hovorun, *Comput. Theor. Chem.*, 2014, **1050**, 15–22.
64 M. W. Freyer and E. A. Lewis, *Biophysical Tools for Biologists, Volume One: In Vitro Techniques*, Academic Press, 2008, vol. 84, pp. 79–113.
65 L. Ferraresso, E. de Arruda, T. de Moraes, R. Fazzi, A. Da Costa Ferreira and C. Abbehausen, *J. Mol. Struct.*, 2017, **1150**, 316–328.
66 L. I. Llarrull, S. M. Fabiane, J. M. Kowalski, B. Bennett, B. J. Sutton and A. J. Vila, *J. Biol. Chem.*, 2007, **282**, 18276–18285.
67 S. Bounaga, A. P. Laws, M. Galleni and M. I. Page, *Biochem. J.*, 1998, **331**, 703–711.
68 C. S. Allen, C.-L. Chuang, M. Cornebise and J. W. Canary, *Inorg. Chim. Acta*, 1995, **239**, 29–37.
69 H. Adams, N. A. Bailey, D. E. Fenton and Q.-Y. He, *J. Chem. Soc., Dalton Trans.*, 1997, 1533–1540.
70 C. Duboc, T. Phoeung, D. Jouvenot, A. G. Blackman, L. F. McClintock, J. Pécaut, M.-N. Collomb and A. Deronzier, *Polyhedron*, 2007, **26**, 5243–5249.
71 J. Morán-Barrio, M.-N. Lisa, N. Larrieux, S. I. Drusin, A. M. Viale, D. M. Moreno, A. Buschiazzo and A. J. Vila, *Antimicrob. Agents Chemother.*, 2016, **60**, 6013–6022.
72 S. Bellais, D. Aubert, T. Naas and P. Nordmann, *Antimicrob. Agents Chemother.*, 2000, **44**, 1878–1886.
73 S. A. V. Jannuzzi, B. Martins, M. I. Felisberti and A. L. B. Formiga, *J. Phys. Chem. B*, 2012, **116**, 14933–14942.
74 M. W. Crowder, J. Spencer and A. J. Vila, *Acc. Chem. Res.*, 2006, **39**, 721–728.
75 M. Umayal, A. Tamilselvi and G. Mugesh, in *Metallo-β-lactamases and their Synthetic Mimics: Structure, Function, and Catalytic Mechanism*, ed. D. K. Karlin, John Willey & Sons, Inc., 2011, pp. 395–443.
76 W. Yang and R. G. Parr, *Proc. Natl. Acad. Sci. U. S. A.*, 1985, **82**, 6723–6726.
77 H. Chermette, *J. Comput. Chem.*, 1999, **20**, 129–154.
78 L. A. Clark, D. E. Ellis and R. Q. Snurr, *J. Chem. Phys.*, 2001, **114**, 2580–2591.
79 P. Fuentealba and C. Cardenas, *Chemical Modelling: Volume 11*, The Royal Society of Chemistry, 2015, vol. 11, pp. 151–174.
80 A. Maynard, M. Huang, W. Rice and D. Covell, *Proc. Natl. Acad. Sci. U. S. A.*, 1998, **95**, 11578–11583.
81 C. Makedonas and C. A. Mitsopoulou, *Eur. J. Inorg. Chem.*, 2006, **2006**, 590–598.
82 Y. Xia, D. Yin, C. Rong, Q. Xu, D. Yin and S. Liu, *J. Phys. Chem. A*, 2008, **112**, 9970–9977.
83 J. Faver and K. M. Merz, *J. Chem. Theory Comput.*, 2010, **6**, 548–559.
84 W. Beker, P. Szarek, L. Komorowski and J. Lipiński, *J. Phys. Chem. A*, 2013, **117**, 1596–1600.
85 R. K. Roy, S. Pal and K. Hirao, *J. Chem. Phys.*, 1999, **110**, 8236–8245.
86 P. Bultinck, R. Carbó-Dorca and W. Langenaeker, *J. Chem. Phys.*, 2003, **118**, 4349–4356.
87 S. Saha, R. K. Roy and P. W. Ayers, *Int. J. Quantum Chem.*, 2009, **109**, 1790–1806.
88 N. Sablon, F. De Proft, P. W. Ayers and P. Geerlings, *J. Chem. Phys.*, 2007, **126**, 224108.
89 F. L. Hirshfeld, *Theor. Chim. Acta.*, 1977, **44**, 129–138.
90 A. E. Reed, R. B. Weinstock and F. Weinhold, *J. Chem. Phys.*, 1985, **83**, 735–746.
91 J. E. Penner-Hahn, *Coord. Chem. Rev.*, 1999, **190–192**, 1101–1123.
92 J. E. Penner-Hahn, *Coord. Chem. Rev.*, 2005, **249**, 161–177.
93 A. Zitolo and P. D′ Angelo, *Chem. Phys. Lett.*, 2010, **499**, 113–116.
94 R. Sarangi, *Coord. Chem. Rev.*, 2013, **257**, 459–472.
95 J. Yuan, J. Wang, G. Zhang, C. Liu, X. Qi, Y. Lan, J. T. Miller, A. J. Kropf, E. E. Bunel and A. Lei, *Chem. Commun.*, 2015, **51**, 576–579.
96 C. Abbehausen, R. E. F. de Paiva, R. Bjornsson, S. Q. Gomes, Z. Du, P. P. Corbi, F. A. Lima and N. Farrell, *Inorg. Chem.*, 2018, **57**, 218–230.
97 M. Roemelt, M. A. Beckwith, C. Duboc, M.-N. Collomb, F. Neese and S. DeBeer, *Inorg. Chem.*, 2011, **51**, 680–687.
98 J. A. Rees, A. Wandzilak, D. Maganas, N. I. Wurster, S. Hugenbruch, J. K. Kowalska, C. J. Pollock, F. A. Lima, K. D. Finkelstein and S. DeBeer, *J. Biol. Inorg. Chem.*, 2016, **21**, 793–805.
99 Y. Chen, E. R. Farquhar, M. R. Chance, K. Palczewski and P. D. Kiser, *J. Biol. Chem.*, 2012, **287**, 13356–13370.
100 M. Silatani, F. A. Lima, T. J. Penfold, J. Rittmann, M. E. Reinhard, H. M. Rittmann-Frank, C. Borca, D. Grolimund, C. J. Milne and M. Chergui, *Proc. Natl. Acad. Sci. U. S. A.*, 2015, **112**, 12922–12927.
101 S. A. V. Jannuzzi, E. G. R. de Arruda, F. A. Lima, M. A. Ribeiro, C. Brinatti and A. L. B. Formiga, *ChemistrySelect*, 2016, **1**, 2235–2243.
102 C. Hennig, F. Thiel, K.-H. Hallmeiér, R. Szargan, A. Hagen and F. Roessner, *Spectrochim. Acta, Part A*, 1993, **49**, 1495–1497.
103 A. L. Dadlani, O. Trejo, S. Acharya, J. Torgersen, I. Petousis, D. Nordlund, R. Sarangi, P. Schindler and F. B. Prinz, *J. Mater. Chem. C*, 2015, **3**, 12192–12198.
104 S. DeBeer George, P. Brant and E. I. Solomon, *J. Am. Chem. Soc.*, 2005, **127**, 667–674.
105 M. A. Beckwith, W. Ames, F. D. Vila, V. Krewald, D. A. Pantazis, C. Mantel, J. Pécaut, M. Gennari,

C. Duboc, M.-N. Collomb, J. Yano, J. J. Rehr, F. Neese and S. DeBeer, *J. Am. Chem. Soc.*, 2015, **137**, 12815–12834.
106 S. M. Mandal, L. Migliolo, O. N. Silva, I. C. M. Fensterseifer, C. Faria-Junior, S. C. Dias, A. Basak, T. K. Hazra and O. L. Franco, *Sci. Rep.*, 2014, **4**, 6015.
107 K. H. M. E. Tehrani and N. I. Martin, *ACS Infect. Dis.*, 2017, **3**, 711–717.
108 S. G. Robinson, P. T. Burns, A. M. Miceli, K. A. Grice, C. E. Karver and L. Jin, *Dalton Trans.*, 2016, **45**, 11817–11829.